doi:10.2533/chimia.2024.297 Chimia 78 (2024) 297–303

Uncovering Atomic-scale Dynamics in Solid Catalysts *via* X-ray-based Methods

Paula Abdala* and Christoph Müller*

Abstract: Deciphering the structural intricacies of catalysts is essential to advance their atomic-scale engineering. Solid catalysts are complex, with structural features spanning multiple length scales and involving dynamics, which possess challenges in understanding structure-performance relationships. However, advanced *operando* X-ray characterization techniques, including X-ray absorption spectroscopy (XAS), diffraction (XRD), and pair distribution function analysis (PDF) allow elucidation of structural features under working conditions, discovering transitions from supported nanocrystals to dispersed sites, from solid solutions to supported nanoparticles, or structural changes at the local level. In this mini-review, we discuss case studies exploring the structure of catalysts over different lengths and time scales under different applications, such as CO_2 hydrogenation to methanol or the dry reforming of methane, using a combination of *operando* XAS, XRD and PDF.

Keywords: *In situ* · *Operando* · Pair distribution function · X-ray absorption · X-ray powder diffraction

Paula M. Abdala obtained a diploma in chemical engineering at UTN-Mendoza, Argentina (2002) and earned her PhD in material science from the Universidad de San Martin, Argentina (2010), studying structure-performance relationships in materials for solid oxide fuel cells. She then moved to France, where she worked as a postdoctoral researcher at the European Synchrotron Radiation Facility. She joined Christoph Müller's group at ETH Zurich, Switzerland, in 2014 where she is currently employed as a senior scientist and lecturer. Her research focuses on understanding structure performance relationships in CO_2 sorbents and catalysts for CO_2 valorization using advanced X-ray based characterization techniques.

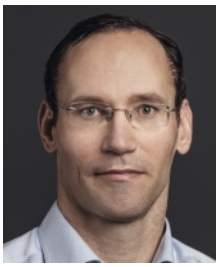

Christoph Müller obtained a diploma in mechanical/process engineering from TU Munich in 2004 and a PhD in chemical engineering from the University of Cambridge in 2008, under the supervision of Prof. John Dennis. In 2010, he became an assistant professor at the department of mechanical and process engineering at ETH Zurich and then in 2018 he became a full professor at the same institution. His research group is active in the development of CO_2 sorbents and catalysts as well as studying single- and multiphase granular flows.

1. Introduction

To achieve global sustainability, it is essential to develop and implement innovative processes that effectively utilize renewable energy sources, raw materials and waste and to establish a circular economy in which products are recycled. Catalysis can play a crucial role in achieving this goal by facilitating chemical transformations required for the production of clean fuels, converting waste into energy, and reducing greenhouse gas emissions, and minimizing waste. Design guidelines for advancing catalysts require an in-depth understanding of the functioning of catalysts.[1]

Heterogeneous solid catalysts are materials that contain a variety of atomic arrangements and chemical species. They have a complex structure that can be defined at multiple scales and undergo structural changes over a wide range of time scales, *i.e.* from sub-milliseconds to years. While catalysis takes place on the surfaces of the material, not the entire surface of the catalyst participates, but only specific centers or active sites. The activity of a catalyst's active site is influenced by geometric and electronic effects which in turn determine the binding strength of the molecular species at the catalyst's surface. Hence, a detailed understanding of the structure of the active sites, both electronic and geometric, is crucial for the design of highly active catalysts with high selectivity towards the desired product(s). However, the complex and dynamic nature of active sites challenges the establishing of structure-performance relationships. Therefore, to engineer active and selective catalysts, it is necessary to understand how the active sites are formed, how these sites respond to different reaction atmospheres and what are the deactivation routes.[1]

The complexities inherent to heterogeneous catalysts call for multi-technique approaches, to probe catalysts at different scales and to enable the characterization of both electronic and geometric features under reactive atmospheres. *Operando* vibrational spectroscopies, such as infrared or Raman are useful to extract detailed information about adsorbed molecules on the catalyst's surface.[2] X-ray techniques such as scattering, absorption, or emission are valuable in studying the structure of catalysts under reaction conditions.[3] When coupled simultaneously with measurements of a catalyst's activity and selectivity, *operando* X-ray based studies allow the catalytic activity to be related to structural features (and changes thereof). In particular, synchrotron-based X-ray techniques have been instrumental in unveiling structural dynamics and addressing questions concerning the structure of complex catalyst systems.[4] Advancing *operando* methods allowing the study of materials with multiple techniques in their working state is a key aspect of catalysis research.

To probe the atomic structure of materials, the combination of X-ray absorption spectroscopy (XAS) and X-ray powder diffraction (XRD) is a powerful approach, irrespective of whether the two techniques are used in the same experimental setup or in two

*Correspondence: Dr. P. M. Abdala, E-mail: abdalap@ethz.ch, Prof. C. Müller, E-mail: muelchri@ethz.ch
Laboratory of Energy Science and Engineering ETH Zurich Leonhardstrasse 21, CH-8092 Zurich, Switzerland.

separate experiments.[3b] XAS allows for the study of the local geometry and electronic state of an atom in a catalyst. This technique encompasses two different formalisms: X-ray absorption near-edge structure analysis (XANES) and X-ray absorption fine structure (EXAFS). XANES provides direct information about the electronic state and coordination geometry of the absorbing element, while EXAFS allows for the quantitative determination of the local atomic structure, described by the coordination number, interatomic distances, and disorder to the nearest neighbors, *i.e.* up to *ca.* 5 Å from the absorbing atom.[3d] In addition, XRD *via* the analysis of Bragg peaks yields quantitative information on the periodic atomic arrangement of the atoms. Moreover, expanding beyond traditional XRD analysis, total scattering techniques such as the pair distribution function (PDF) analysis have emerged as important tools for probing the structure of materials across different length scales, *i.e.* from the local atomic environment to the mid-range structure (a few Angstroms to several nanometres).[5] Fig. 1 illustrates the complementary information accessible by XAS (XANES and EXAFS), XRD and PDF analyses under *operando* or *in situ* conditions.

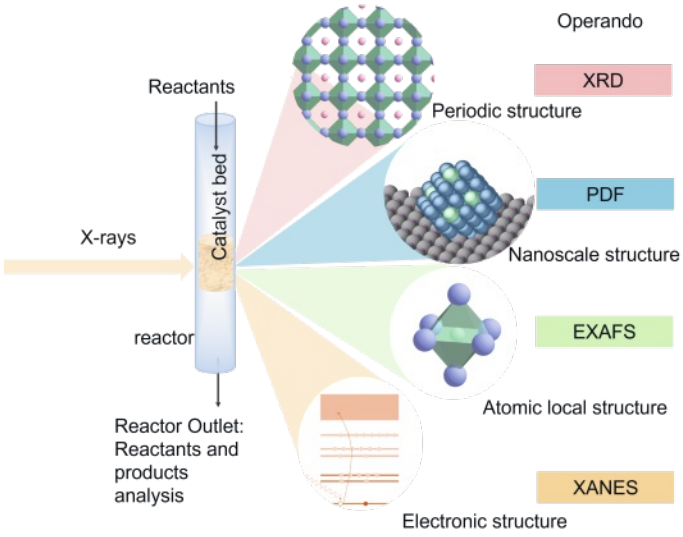

Fig. 1. Schematic overview of *operando* complementary X-ray-based techniques and the underlaying information that can be extracted from them.

In this mini-review, we will discuss how XAS, XRD, and PDF can provide information to understand in more detail the relationship between the structure and performance of solid catalysts, as well as elucidate their structural (activation or deactivation) dynamics. We will focus on research conducted in the Laboratory of Energy Science and Engineering at ETH Zurich, Switzerland which focuses on the examination of structural changes of catalysts under various reactive conditions. The investigations highlighted here have allowed a fundamental understanding of emerging catalyst systems that hold promise for applications in sustainable catalysis to be obtained, in particular in catalytic reactions that are concerned with CO_2 valorization.

2. Tracking Transformations in Solid Catalysts Using Combined XAS-XRD

The combination of time resolved XAS and XRD techniques, applied under reaction conditions, have proven to be crucial to establish structure-performance relationships in solid catalysts.[3b,4b,4e,6] The combination of these two techniques provided information concerning changes occurring in the electronic, local, and average crystalline structure of catalysts under reactive atmospheres. By using *operando* XAS-XRD techniques, researchers have been able to correlate these changes to the catalyst's performance.[4a,c]

2.1 *From Nanocrystals to Atomically Dispersed Sites*

The direct conversion of CO_2 to alcohols, such as methanol, is a promising route to produce platform chemicals and energy carriers. Various catalysts are being explored for this process, including metals, metal oxides, and intermetallic compounds; the design of catalysts' of increased activity depends critically on an in-depth understanding of the active sites and the prevailing deactivation mechanisms.[4g,7] For instance, Tsoukalou *et al.* have combined XAS with XRD under *operando* conditions to provide insight into the structure-activity relationship of an In_2O_3-based catalyst for CO_2 hydrogenation to methanol.[4c] Here, In_2O_3 nanocrystals of 7 nm in diameter with a bixbyite type structure were synthesized *via* a colloidal route which acted as a model system. The study monitored changes in the local structure, oxidation state of In, and nanoscale structure of these nanocrystals under CO_2 hydrogenation conditions (300 °C, 20 bar, H_2:CO_2:N_2 = 3:1:1) *via* XAS-XRD coupled with an effluent gas analysis using a gas chromatograph (GC).[4c] The *operando* experiments were carried out at the BM31 station of the Swiss Norwegian Beamlines, SNBL.[3b,8] The results showed that an initial activation stage involved the formation of oxygen vacancy sites associated with a partial reduction of indium, leading to the active state In_2O_{3-x}. Subsequently, as the reaction progressed, reductive amorphization of the In_2O_3 nanocrystals occurred, revealed through quantitative XANES, EXAFS, and XRD analyses (Fig 2a-d). A multivariate curve resolution-alternating least squares (MCR-ALS) analysis applied to the XANES data indicated that the most active catalyst state has an average oxidation state between +3 and +2 while the onset of deactivation coincided with the appearance of molten In^0 (Fig 2a-b). The over-reduction of In_2O_3 with time on stream (TOS) led to a In^0/In_2O_{3-x} material of inferior catalytic activity. Indeed, the decrease in In-O and In-In coordination numbers determined by EXAFS were interpreted as a reductive amorphization of the In_2O_3 nanocrystals (Fig 2c). XRD analysis provided further evidence for the amorphization processes and allowed the quantification of the degree of amorphization using BN as an internal standard (Fig 2c). Hence, these findings indicate that it is essential to implement strategies to prevent the over-reduction of indium oxide during reaction.

In a subsequent investigation, the researchers deposited In_2O_3 nanocrystals onto different ZrO_2 supports, *i.e.* monoclinic (In_2O_3/m-ZrO_2), tetragonal (In_2O_3/t-ZrO_2) and amorphous (In_2O_3/am-ZrO_2).[4a] The three different catalyst systems were probed by *operando* XAS-XRD to determine whether the different ZrO_2 phases affected the oxidation state and coordination environment of the In atoms. The goal of the *operando* study was to assess how structural differences between the catalysts correlate with their catalytic activity, selectivity, and stability. Interestingly, In_2O_3/m-ZrO_2 showed a significantly higher performance in terms of methanol yield and stability when compared to In_2O_3/t-ZrO_2 and In_2O_3/am-ZrO_2. XAS-XRD analysis revealed that the phase of the ZrO_2 support played a crucial role in determining the structural evolution of the In_2O_3 nanocrystals during reaction. In the In_2O_3/m-ZrO_2 system, In^{2+}/In^{3+} sites were effectively stabilized, as evidenced by XANES. EXAFS showed that the stabilization of the oxidation state was linked to a structural transformation that turned nanocrystals into In sites that were highly dispersed in the monoclinic ZrO_2 structure, forming a solid solution. The formation of a solid solution prevented the over-reduction of In^{2+}/In^{3+} sites to metallic In *via* the formation of highly active and stable In–Vo–Zr linkages (Vo is an oxygen vacancy). In contrast, the amorphous or tetragonal zirconia supports did not yield a solid solution with In_2O_3 and as a result, In_2O_3/am-ZrO_2 and In_2O_3/t-

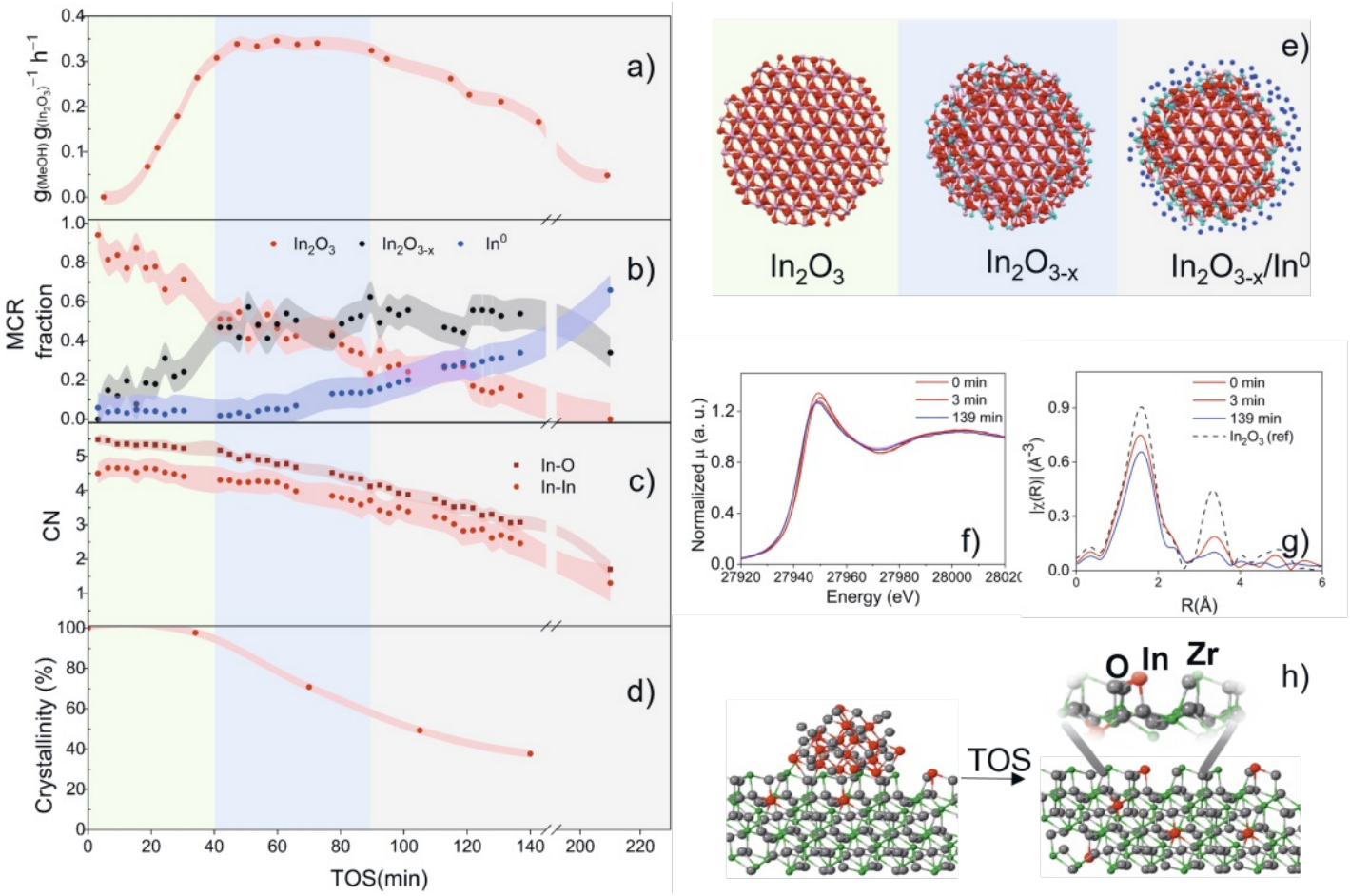

Fig. 2. a) Methanol production rate; b) MCR-ALS analysis and c) fitted In–O and In–In coordination numbers d) fraction of crystalline bcc-In_2O_3 and e) an illustration of the transformation of In_2O_3 nanocrystals during an *operando* CO_2 hydrogenation experiment as a function of TOS. Adapted with permission from ref. [4c] Copyright **2019** *American Chemical Society*. f) XANES, g) Fourier transformed EXAFS data and h) an illustration of the transformation of In_2O_3/m-ZrO_2 during CO_2 hydrogenation. Adapted with permission from ref. [4a] Copyright **2020** *American Chemical Society.*

ZrO_2 reduced to In^0 under reaction conditions explaining in turn their inferior performance.

These two examples show how a combination of advanced techniques such as *operando* XAS-XRD, is able to probe structural dynamics during CO_2 hydrogenation conditions, providing valuable insights into the active state and deactivation routes, which in turn allowed the development of stabilization strategies.

2.2 *From Solid Solutions to Supported Nanoparticles*

In addition to the hydrogenation of CO_2 to methanol, the dry reforming of methane (DRM) is also a promising route to valorize CO_2. DRM converts methane (CH_4) and carbon dioxide (CO_2) into synthesis gas, *i.e.* a mixture of CO and H_2 which is an essential feedstock for various industrial processes, such as the production of synthetic fuels. A key challenge of DRM is the development of stable catalysts.[4b,d,9] In fact, under the harsh DRM conditions (600 – 900 °C) catalysts deactivate through a series of routes such as coke deposition, oxidation of the active phase or sintering.[4d,9] Noble metals (*e.g.* Pt, Ru, Rh) based catalysts often show resilience against coking and oxidation, yet their high costs necessitate an optimized metal usage.[9b] Therefore, it is crucial to develop approaches that yield supported noble-metal-based DRM catalysts with a high surface to volume ratio enabling the minimizing of the noble metal content. In this context, the reductive exsolution has established itself as a promising approach to yield highly dispersed, metallic or bimetallic nanoparticles that are supported on a metal oxide matrix.[10] Reductive exsolution exploits the segregation of a metal from a host oxide when exposed to a reductive atmosphere. Typically, the host structure is a perovskite (ABO_3) where a late transition metal replaces the B site metal, but alternative structures such as fluorite or rock salt-type have also been utilized.[4b,10,11] Naeem *et al.* explored reductive exsolution of Ru from fluorite-type solid solutions $Sm_2Ru_xCe_{2-x}O_7$ to obtain catalysts with a high activity and stability for DRM and to shed light on their structural dynamics through the application of *in situ*/*operando* XAS-XRD.[4b] It was observed, that after 100 h of TOS at 700 °C, the exsolved catalysts deactivated by only ~1% while a benchmark catalyst prepared by conventional wetness impregnation (denoted Ru/$Sm_2Ce_2O_7$-Imp), lost *ca.* 8% of the initial activity after only 48 h of TOS.

An effective exsolution process requires a precursor material in which Ru cations (Ru^{+4}) are homogeneously incorporated into a metal oxide matrix forming a solid solution. Therefore, a vital step was the preparation of phase pure, $Sm_2Ru_xCe_{2-x}O_7$ solid solutions (where x = 0, 0.1, 0.2, 0.4) and their in-depth structural characterization using XRD and XAS, in addition to complementary techniques, including *ex situ* scanning transmission electron microscopy (STEM) and Raman spectroscopy. The $Sm_2Ce_2O_7$ crystal structure is described as a C-type (space group *Ia*-3), which is a superstructure of a fluorite-type structure. The C-type atomic arrangement contains two oxygen positions (48e and 16c), with oxygen vacancies preferentially located at the 16c site. The structure contains two cation sites (8b and 24d) which are randomly occupied by Sm and Ce atoms. As Ru is gradually incorporated into the cationic sites of the solid solutions, the material transforms into a type of defective fluorite, in which oxygen vacancies are randomly located at the fluorite oxygen site (8c). This transformation was revealed through changes in the synchrotron-based

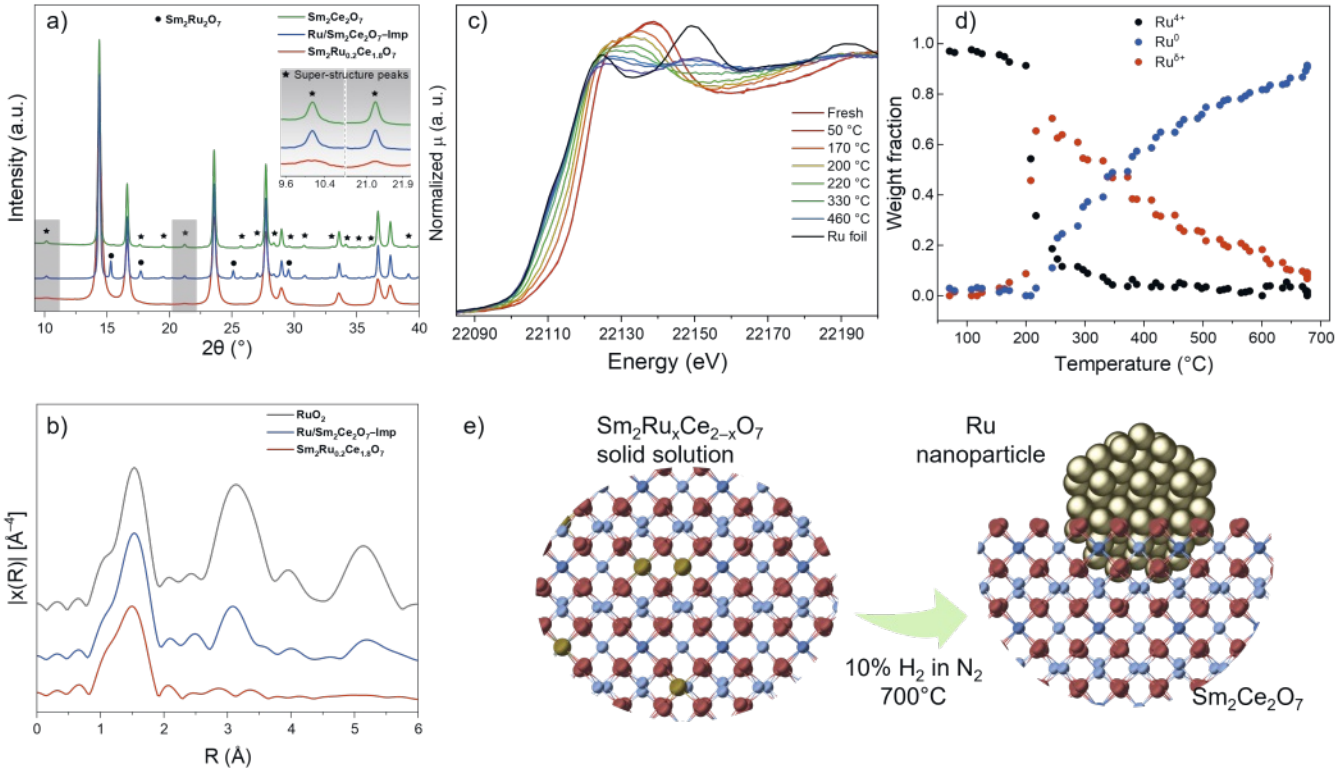

Fig. 3. a) XRD patterns (λ = 0.78956 Å) of $Sm_2Ce_2O_7$, $Sm_2Ru_{0.2}Ce_{1.8}O_7$, and Ru/$Sm_2Ce_2O_7$-Imp. b) Fourier transform of the Ru K-edge EXAFS of $Sm_2Ru_{0.2}Ce_{1.8}O_7$, Ru/$Sm_2Ce_2O_7$-Imp and RuO_2. Adapted with permission from ref. [4b] Copyright **2019** *American Chemical Society*. c) Ru K-edge XANES spectra collected during an *in situ* TPR experiment (conditions 10% H_2 in N_2) and d) corresponding MCR-ALS analysis. e) Illustration of the exsolution process. Adapted with permission from ref. [6c] Copyright **2020** *American Chemical Society*.

diffraction patterns, showing that the relatively weak peaks due to superstructures in the C-type phase gradually vanished upon the substitution of Ru into $Sm_2Ce_2O_7$ (Fig. 3a).

Further, Ru K-edge XAS was utilized to probe the local environment around the Ru atoms in the solid solutions. EXAFS analysis revealed the presence of an Ru–O shell in the solid solution, while no higher coordination spheres were observed. This contrasted the EXAFS data of RuO_2 or the benchmark catalysts Ru/$Sm_2Ce_2O_7$-Imp, which exhibit well-defined second Ru-metal spheres (Fig. 3b). The EXAFS data of $Sm_2Ru_xCe_{2-x}O_7$ solid solutions did not show any second shell peak because the backscattering signals from Sm and Ce atoms interfere destructively and point to a local disorder around Ru in these solid solutions. In line with the EXAFS analyses, XANES data shows features in $Sm_2Ru_xCe_{2-x}O_7$ that are distinct with respect to the reference RuO_2 suggesting a unique environment of Ru in $Sm_2Ru_xCe_{2-x}O_7$.

An *in situ* combined XRD-XAS (Ru K-edge) experiment provided further insight into the structural evolution of $Sm_2Ru_{0.2}Ce_{1.8}O_7$ under reductive exsolution conditions (10 vol % H_2 in N_2) when heated up from 25 and 700 °C.[4b,6c] The gradual reduction of Ru^{+4} to Ru^0 was evidenced by the decrease in the white line intensity and the shift of the absorption edge to lower energies (Fig. 3c). Principal component analysis (PCA) and MCR-ALS applied to the *in situ* XANES data allowed the evolution of the oxidation state of Ru during reduction to be resolved in time (Fig 3b). This analysis evidenced that Ru exsolves from the parent solid solution through an intermediate $Ru^{\delta+}$ state, that is $Ru^{4+} \rightarrow Ru^{\delta+} \rightarrow Ru^0$. EXAFS analysis revealed that the Ru–O interatomic distances increase from 1.96 to 2.02 Å during the formation of the intermediate $Ru^{\delta+}$ state. Moreover, the EXAFS analysis evidenced a developing Ru-Ru sphere due to Ru^0 nanoparticle formation starting at *ca.* 500 °C. The XRD data further shows the emergence of C-type reflections due to an oxygen vacancy ordering in $Sm_2Ce_2O_7$, indicating that the exsolution of Ru from $Sm_2Ru_{0.2}Ce_{1.8}O_7$ triggers a fluorite-to-C-type transition. By modelling of the EXAFS data (data collected at 50 °C), the first sphere Ru-Ru coordination number was determined as 6, which indicated the formation of Ru nanoparticles of *ca.* 1-1.5 nm in diameter, in line with *ex situ* scanning transmission electron microscopy (STEM). Notably the Ru–Ru coordination number of a material prepared *via* a conventional impregnation approach (Ru/$Sm_2Ce_2O_7$-Imp) was *ca.* 10 confirming that impregnation led to significantly larger Ru particle sizes (*i.e.* 3-4 nm). An illustration of the reductive exsolution process is shown in Fig. 3e.

Under DRM conditions, *operando* XAS-XRD coupled with mass spectrometry confirmed the absence of changes in the oxidation state or structure of Ru over 1.5 h on TOS; further, no deactivation was observed by the off-gas analysis. However, EXAFS analysis (50°C) of the reacted catalysts indicated a slight increase in the coordination number from 6 to 7, a possible indication of a small growth of the Ru nanoparticles, yet this increase was within the experimental error. Although no detectable catalyst deactivation occurred, particle growth over longer TOS cannot be ruled out. Therefore, the cyclic reversibility of the exsolution-redissolution processes was investigated using an oxidative atmosphere (20 vol % O_2 in N_2 at 700 °C) as a regeneration route. This redissolution process was followed by Ru K-edge XAS which showed that the material completely recovered all of the characteristic features of the freshly calcined material in less than 10 min, suggesting that the Ru exsolution-dissolution process is indeed reversible.[4b]

These studies demonstrate how XAS-XRD can aid in developing high-performance catalysts and reliable regeneration procedures.

3. Probing Changes at the Nanoscale Using PDF Analysis

Traditional crystallographic methods have limitations in providing detailed and quantitative structural information on small nanoparticles and nanocrystals. This is because the Bragg diffraction peaks broaden due to the short coherence length and frequent-

ly defective structures. As a result, diffuse scattering dominates the scattering patterns. PDF analysis is suitable for the analysis of nanostructured and defective materials as it utilizes the entire information contained in the diffraction pattern by considering both the Bragg peaks and diffuse scattering.[5b,c] It provides the probability of finding pairs of atoms separated by a distance r, and thus offers direct insight into the short- and intermediate-range order of materials. PDF bridges the gap between the structural length scales accessible by diffraction methods (> *ca.* 5 nm) and EXAFS (< *ca.* 6 Å). PDF data is derived experimentally from X-ray total scattering patterns (optimized for high scattering vector with Q > 15 $Å^{-1}$, using high energy photons) *via* a Fourier transformation. PDF can probe structures at multiple length scales from a few Å to several nm, making it an ideal method to study the structures of catalysts at multiple scales and complementing XAS. There is a growing number of applications of PDF in catalysis research including temporally resolved PDF.[5a]

3.1 *Uncovering Transformations Occurring on Different Length Scales in Ga_2O_3 Nanocrystals*

Nanocrystalline materials can stabilize defects and metastable phases, which might possess properties different to those of larger crystals.[5b,12] In nanocrystalline materials, the high surface energy and strain associated with the high density of grain boundaries can stabilize metastable phases. For instance, metastable γ-Ga_2O_3 nanocrystals have received increasing interest for different (electro)catalytic applications. PDF analysis in combination with XAS and ^{71}Ga solid-state magic-angle spinning nuclear magnetic resonance (MAS NMR) was key to describe the structure and to unveil disorder in small metastable γ-Ga_2O_3 nanocrystals (2.5 nm).[12b] PDF uncovered that the local structure (< 8 Å) of these γ-Ga_2O_3 nanocrystals deviates from the average cubic spinel-type structure due to a high degree of disorder.[12b,13] The disorder arises from a distortion of the Ga-O polyhedra, which are randomly oriented within the nanocrystal. Castro-Fernández *et al.* using *in situ* time resolved PDF, showed that the transformation of the γ-Ga_2O_3 nanocrystals towards the thermodynamically stable β-Ga_2O_3 polymorph occurs in different structural domains.[13] The study revealed the appearance of sub-nanometric β-Ga_2O_3 domains at approximately 300 °C, while the bulk γ→β-Ga_2O_3 transition occurs at a much higher temperature (600-750 °C), which may have implications for their photo/thermal catalytic performance.

Moreover, PDF can be used to probe the structure of supported nanoparticles or films; an important aspect, because in catalytic applications the active phase is often dispersed on high surface area materials (supports) to prevent or at least minimize their agglomeration and sintering during operation. To study the structure of supported phases, the PDF signal of the support is subtracted from the total PDF, resulting in a differential (d-PDF).[5a] For example, the d-PDF approach has been used to characterize the structure of SiO_2-supported GaO_x catalysts that were synthesized using different methods, *viz.* colloidal based approaches, wetness impregnation of aqueous $Ga(NO_3)_3$ solutions, and atomic layer deposition.[14] By combining XAS at the Ga K-edge and ^{71}Ga MAS NMR that provided information of the local Ga coordination with d-PDF it was possible to characterize the local structure and coherence length of the differently prepared GaO_x/SiO_2 catalysts and allowed to correlate their structural specifics with their catalytic activity in propane dehydrogenation (PDH).[14b]

3.2 *Bimetallic Nanoparticles and the Cooperativity of Alloyed and Oxidic Species*

A versatile strategy to tune the catalytic properties of a metal nanoparticle is to add a second metal. This typically alters the electronic and, or the geometric structure of the catalyst surface, modifying in turn its catalytic properties.[3a,4d,g,15] Understanding the role of the secondary metal (or promoter) is key to designing effective catalysts.[4g] For example, Ni-based catalysts are very effective in the methanation reaction, while the addition of Ga to Ni has shown a shift in its selectivity towards methanol.[16] Zimmerli *et al.* conducted research to understand the role and structure of Ga as a promoter in Ni-based catalysts for the hydrogenation of CO_2 to methanol.[17] To this end, a series of Ni-Ga-based catalysts with different Ni:Ga ratios (Ni_{100}/SiO_2, $Ni_{75}Ga_{25}/SiO_2$, $Ni_{70}Ga_{30}/SiO_2$ and $Ni_{65}Ga_{35}/SiO_2$) were synthesized using surface organometallic chemistry (SOMC)[18] and the structure of the catalysts were interrogated using *operando* d-PDF and *operando* XAS.[17]

In this research d-PDF analysis was critical to provide atomic-level insight of the structure of the very small (2 nm) nanoparticles formed (Fig. 4 a,b). It was found that when activated at 600 °C in H_2, nanoparticles of an Ni_xGa_y alloy with an fcc structure and a size of approximately 2 nm formed. Using the cell parameters determined by d-PDF refinements, it was possible to determine the composition of the alloys (Fig 4 c). Additionally, the quantity of GaO_x species were estimated by taking into account the total Ga and Ni contents determined by inductively coupled plasma optical emission spectroscopy (ICP-OES). The results obtained by *in situ* XAS at the Ga K-edge confirmed the presence of oxidic Ga species while Ni K-edge XANES indicated that the electronic structure of Ni is changed upon the addition of Ga, *viz.* there is a charge transfer from Ga to Ni ($Ga^{\delta+}/Ni^{\delta-}$). Additional *operando* d-PDF and XAS experiments of the catalysts under CO_2 hydrogenation conditions (20 bar CO_2:H_2:N_2 = 1:3:1, 230 °C) showed that the structure of the catalysts formed after activation was maintained under reaction conditions, *i.e.* the quantities of the alloyed Ga and GaO_x species remained constant with TOS.

When correlating catalytic activity and structural descriptors, it was discovered already that the alloying of very small amounts of Ga with Ni (Ni:Ga ratio = 82:12) resulted in a significant selectivity shift from methane to methanol under CO_2 hydrogenation conditions. The most active and selective catalyst of the series studied (*i.e.* $Ni_{65}Ga_{35}/SiO_2$) contained an alloy with a Ni:Ga ratio of 75:25 and GaO_x species (0.14 mol_{GaOx} $mol_{Ni^{-1}}$) (Fig. 4d-e). In addition, monitoring the catalysts by *operando* diffuse reflectance infrared Fourier transform spectroscopy (DRIFTS) provided insight into the surface species under reaction conditions. It is worth noting that only the most active catalyst showed bands due to formate species. Combining the findings of *operando* d-PDF, XAS and DRIFTS, the authors concluded that the alloying of Ni with Ga is crucial for achieving high methanol selectivity, while the presence of oxidized Ga species appreciably enhances the rate of methanol formation. Alloy nanoparticles with a Ni:Ga ratio of 75:25 result in the high methanol activity and selectivity, considerably surpassing the performance of Ni-richer alloys, while the presence of GaO_x further increases the rate of methanol formation.

To summarize, in this work the combination of *operando* X-ray-based techniques and infrared spectroscopy provided atomic-scale insight in the geometric and electronic structure of ultra-small nanoparticles (2 nm) that is crucial for the advancement of Ni-Ga-based bimetallic catalysts for CO_2 hydrogenation. Further, the study highlighted that regulating the quantity of both alloyed Ga and GaO_x species is crucial in achieving high methanol selectivity and a high rate of methanol formation.

4. Conclusions and Outlook

Advanced *operando* X-ray-based characterization techniques play a crucial role in advancing our understanding of the complex dynamics of solid catalysts at the atomic- and nano-scale. In this mini-review, where we highlight recent advances of our group with regards to *operando* synchrotron XAS, XRD and PDF analyses, we present a number of diverse case studies of catalysts for the hydrogenation of CO_2 to methanol, dry reforming of methane,

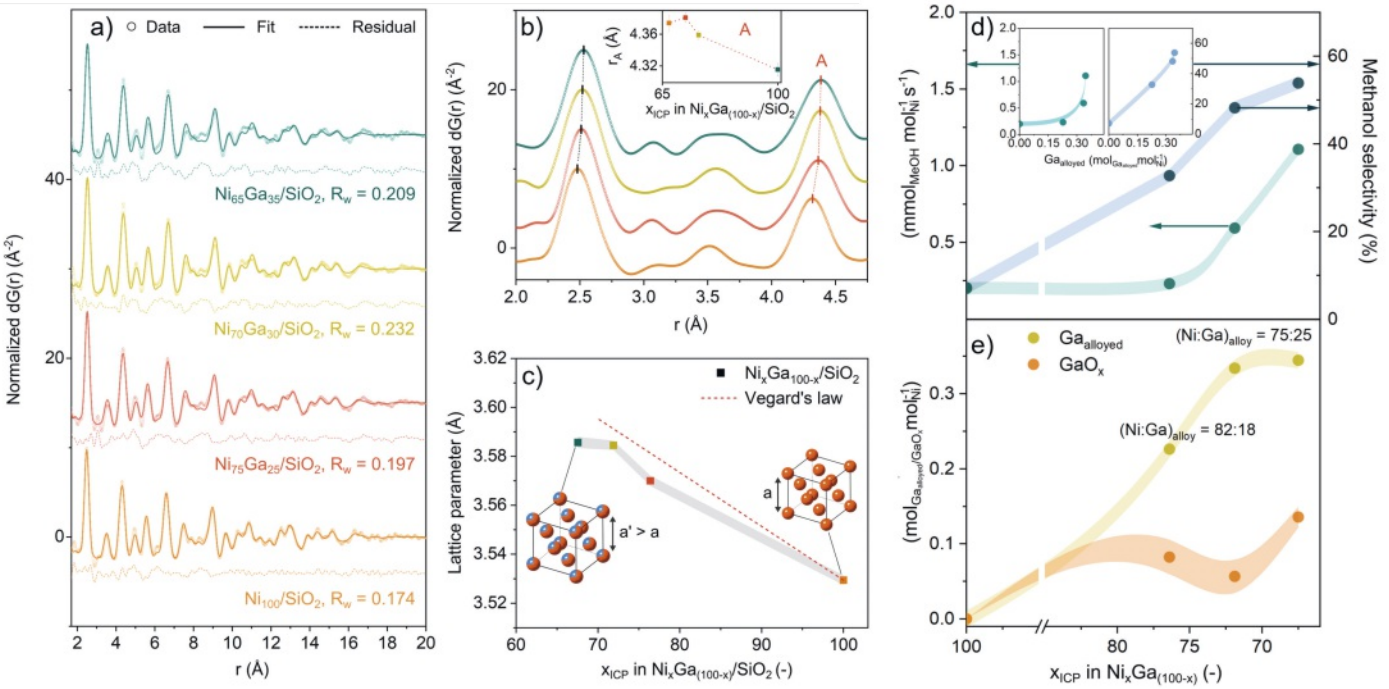

Fig. 4. a) d-PDF data fitted to a fcc-$Ni_yGa_{(100-y)}$ alloy and the corresponding agreement factors (R_w) at 1 bar H_2, 230 °C, after *in situ* activation. b) Zoom into the region r = 2-4.75 Å of the d-PDF data and the fitted position of the metal-metal pair correlation labelled A as a function of x_{ICP} in the catalysts. c) Lattice parameter as a function of the fraction of Ni. d) Product formation rates over $Ni_xGa_{(100-x)}/SiO_2$ and e) methanol formation rate and methanol selectivity as a function of x_{ICP} in $Ni_xGa_{(100-x)}/SiO_2$ as determined by ICP. Reproduced from ref. [17].

and propane dehydrogenation. These case studies demonstrate the value of XAS, XRD, and PDF to formulate correlations between a catalyst's structure and its catalytic performance. *Operando* and *in situ* XAS and XRD techniques provide structural information over multiple length scales, ranging from the atomic to the nm-scale. Specifically, XAS provides element-specific information of the local and electronic structure around the element being investigated, while XRD yields insight concerning the average structure that extends to several nanometers or even micrometers. In addition, PDF analysis bridges the gap between XAS and XRD and provides structural information (although not being element specific) across several length scales and is particularly suited for amorphous materials or very small nanoparticles. *In situ*, *operando* and transient experiments using X-ray-based techniques are valuable for deciphering structural dynamics and hence to elucidate catalyst activation and/or deactivation mechanisms.

In summary, the cooperative use of XAS, XRD, and PDF techniques will contribute significantly in untangling the complex relationships between structure and performance in solid catalysts. In turn, this understanding can be utilized to improve catalyst formulations and mitigate their deactivation. In the future, it will be important to advance further the development of tailored setups that combine these techniques under reaction conditions, offering analyses that are time resolved and integrated with additional methods such as small-angle X-ray scattering to gain insight into the nanoparticle morphology and changes thereof.

Acknowledgements

This publication was created as part of NCCR Catalysis (grant number 180544), a National Centre of Competence in Research funded by the Swiss National Science Foundation. The Swiss Norwegian beamlines (SNBL) and the ESRF are acknowledged for the provision of the beamtime. The Swiss National Science Foundation (grant 20602118629) is thanked for providing equipment for the upgrade of the SNBL facilities.

Received: January 09, 2024

[1] C. Vogt, B. M. Weckhuysen, *Nat. Rev. Chem.* **2022**, *6*, 89, https://doi.org/10.1038/s41570-021-00340-y.

[2] E. Groppo, S. Rojas-Buzo, S. Bordiga, *Chem. Rev.* **2023**, *123*, 12135, https://doi.org/10.1021/acs.chemrev.3c00372

[3] a) M. Filez, E. A. Redekop, J. Dendooven, R. K. Ramachandran, E. Solano, U. Olsbye, B. M. Weckhuysen, V. V. Galvita, H. Poelman, C. Detavernier, *Angew. Chem. Int. Ed.* **2019**, *58*, 13220, https://doi.org/10.1002/anie.201984411; b) P. M. Abdala, O. V. Safonova, G. Wiker, W. V. Beek, H. Emerich, J. A. V. Bokhoven, J. Sá, J. Szlachetko, M. Nachtegaal, *CHIMIA* **2012**, *66*, 699, https://doi.org/ 10.2533/chimia.2012.699; c) W. van der Stam, *Chem. Mater.* **2023**, *35*, 386, https://doi.org/10.1021/acs.chemmater.2c03286; d) J. A. Van Bokhoven, C. Lamberti, 'X-ray absorption and X-ray emission spectroscopy: theory and applications', Vol. 1, John Wiley & Sons, **2016**.

[4] a) A. Tsoukalou, P. M. Abdala, A. Armutlulu, E. Willinger, A. Fedorov, C. R. Müller, *ACS Catal.* **2020**, *10*, 10060, https://doi.org/10.1021/acscatal.0c01968; b) M. A. Naeem, P. M. Abdala, A. Armutlulu, S. M. Kim, A. Fedorov, C. R. Müller, *ACS Catal.* **2020**, *10*, 1923, https://doi.org/10.1021/acscatal.9b04555; c) A. Tsoukalou, P. M. Abdala, D. Stoian, X. Huang, M. G. Willinger, A. Fedorov, C. R. Müller, *J. Am. Chem. Soc.* **2019**, *141*, 13497, https://doi.org/10.1021/jacs.9b04873; d) S. M. Kim, P. M. Abdala, T. Margossian, D. Hosseini, L. Foppa, A. Armutlulu, W. van Beek, A. Comas-Vives, C. Copéret, C. Müller, *J. Am. Chem. Soc.* **2017**, *139*, 1937, https://doi.org/10.1021/jacs.6b11487; e) M. Nadjafi, A. M. Kierzkowska, A. Armutlulu, R. Verel, A. Fedorov, P. M. Abdala, C. R. Müller, *J. Phys. Chem. C* **2021**, *125*, 14065, https://doi.org/10.1021/acs.jpcc.1c03175; f) A. Zabilska, M. Zabilskiy, R. J. G. Nuguid, A. H. Clark, I. I. Sadykov, M. Nachtegaal, O. Kröcher, O. V. Safonova, *Angew. Chem. Int. Ed.* **2023**, *135*, e202301297, https://doi.org/10.1002/ange.202301297; g) S. R. Docherty, N. Phongprueksathat, E. Lam, G. Noh, O. V. Safonova, A. Urakawa, C. Copéret, *JACS Au* **2021**, *1*, 450, https://doi.org/10.1021/jacsau.1c00021.

[5] a) N. K. Zimmerli, C. R. Müller, P. M. Abdala, *Trends Chem.* **2022**, *4*, 807, https://doi.org/10.1016/j.trechm.2022.06.006; b) T. L. Christiansen, S. R. Cooper, K. M. Jensen, *Nanoscale Adv.* **2020**, *2*, 2234, https://doi.org/10.1039/D0NA00120A; c) K. M. Jensen, *CHIMIA* **2021**, *75*, 368, https://doi.org/10.2533/chimia.2021.368; d) T. Egami, S. J. Billinge, 'Underneath the Bragg peaks: structural analysis of complex materials', Elsevier, **2003**; e) J. A. Kaduk, S. J. L. Billinge, R. E. Dinnebier, N. Henderson, I. Madsen, R. Černý, M. Leoni, L. Lutterotti, S. Thakral, D. Chateigner, *Nat. Rev. Methods Primers* **2021**, *1*, 77, https://doi.org/10.1038/s43586-021-00074-7.

[6] a) R. Pereñíguez, D. Ferri, *ChemPhysChem* **2018**, *19*, 1876, https://doi.org/10.1002/cphc.201800069; b) N. E. Tsakoumis, J. C. Walmsley, M. Rønning, W. van Beek, E. Rytter, A. Holmen, *J. Am.*

Chem. Soc. **2017**, *139*, 3706, https://doi.org/10.1021/jacs.6b11872; c) M. A. Naeem, D. B. Burueva, P. M. Abdala, N. S. Bushkov, D. Stoian, A. V. Bukhtiyarov, I. P. Prosvirin, V. I. Bukhtiyarov, K. V. Kovtunov, I. V. Koptyug, A. Fedorov, C. R. Müller, *J. Phys. Chem. C* **2020**, *124*, 25299, https://doi.org/10.1021/acs.jpcc.0c07203.

[7] a) X. Jiang, X. Nie, X. Guo, C. Song, J. G. Chen, *Chem. Rev.* **2020**, *120*, 7984, https://doi.org/ 10.1021/acs.chemrev.9b00723; b) O. Martin, A. J. Martin, C. Mondelli, S. Mitchell, T. F. Segawa, R. Hauert, C. Drouilly, D. Curulla-Ferre, J. Perez-Ramirez, *Angew. Chem. Int. Ed.* **2016**, *55*, 6261, https://doi.org/10.1002/anie.201600943.

[8] P. M. Abdala, H. Mauroy, W. Van Beek, *J. Appl. Crystallogr.* **2014**, *47*, 449, https://doi.org/10.1107/S1600576713034067.

[9] a) A. Kurlov, X. Huang, E. B. Deeva, P. M. Abdala, A. Fedorov, C. R. Müller, *Nanoscale* **2020**, *12*, 13086, https://doi.org/10.1039/D0NR02908D; b) D. Pakhare, J. Spivey, *Chem. Soc. Rev.* **2014**, *43*, 7813, https://doi.org/10.1039/C3CS60395D.

[10] D. Neagu, T.-S. Oh, D. N. Miller, H. Ménard, S. M. Bukhari, S. R. Gamble, R. J. Gorte, J. M. Vohs, J. T. S. Irvine, *Nat. Commun.* **2015**, *6*, 8120, https://doi.org/10.1038/ncomms9120.

[11] Y. S. Park, M. Kang, P. Byeon, S.-Y. Chung, T. Nakayama, T. Ko, H. Hwang, *J. Power Sources* **2018**, *397*, 318, https://doi.org/10.1016/j.jpowsour.2018.07.025.

[12] a) P. M. Abdala, A. F. Craievich, M. C. Fantini, M. L. Temperini, D. G. Lamas, *J. Phys. Chem.* **2009**, *113*, 18661, https://doi.org/10.1021/jp904584e; b) H. Y. Playford, A. C. Hannon, M. G. Tucker, D. M. Dawson, S. E. Ashbrook, R. J. Kastiban, J. Sloan, R. I. Walton, *J. Phys. Chem. C* **2014**, *118*, 16188, https://doi.org/10.1021/jp5033806.

[13] P. Castro-Fernández, M. V. Blanco, R. Verel, E. Willinger, A. Fedorov, P. M. Abdala, C. R. Müller, *J. Phys. Chem.* **2020**, 124, *37*, 20578, https://doi.org/10.1021/acs.jpcc.0c05885.

[14] a) P. Castro-Fernández, D. Mance, C. Liu, P. M. Abdala, E. Willinger, A. A. Rossinelli, A. I. Serykh, E. A. Pidko, C. Copéret, A. Fedorov, C. R. Müller, *J. Catal.* **2022**, *408*, 155, https://doi.org/10.1016/j.jcat.2022.02.025; b) P. Castro-Fernández, D. Mance, C. Liu, I. B. Moroz, P. M. Abdala, E. A. Pidko, C. Copéret, A. Fedorov, C. R. Müller, *ACS Cat.* **2021**, *11*, 907, https://doi.org/10.1021/acscatal.0c05009; c) Z. Chen, N. K. Zimmerli, M. Zubair, A. V. Yakimov, S. s. Björgvinsdóttir, N. Alaniva, E. Willinger, A. B. Barnes, N. M. Bedford, C. Copéret, *Chem. Mat.* **2023**, *35*, 7475, https://doi.org/10.1021/acs.chemmater.3c00923.

[15] a) A. Tsoukalou, Q. Imtiaz, S. M. Kim, P. M. Abdala, S. Yoon, C. R. Müller, J. Catal. 2016, 343, 208, https://doi.org/10.1016/j.jcat.2016.03.018; b) Z. Bian, S. Das, M. H. Wai, P. Hongmanorom, S. Kawi, *ChemPhysChem* **2017**, *18*, 3117, https://doi.org/10.1002/cphc.201700529; c) D. Liu, Y. Li, M. Kottwitz, B. Yan, S. Yao, A. Gamalski, D. Grolimund, O. V. Safonova, M. Nachtegaal, J. G. Chen, *ACS Catal.* **2018**, *8*, 4120, https://doi.org/10.1021/acscatal.8b00706.

[16] a) A. Gallo, J. L. Snider, D. Sokaras, D. Nordlund, T. Kroll, H. Ogasawara, L. Kovarik, M. S. Duyar, T. F. Jaramillo, *Appl. Catal. B: Envir.* **2020**, *267*, 118369, https://doi.org/10.1016/j.apcatb.2019.118369; b) F. Studt, I. Sharafutdinov, F. Abild-Pedersen, C. F. Elkjær, J. S. Hummelshøj, S. Dahl, I. Chorkendorff, J. K. Nørskov, *Nat. Chem.* **2014**, *6*, 320, https://doi.org/10.1038/nchem.1873.

[17] N. K. Zimmerli, L. Rochlitz, S. Checchia, C. R. Müller, C. Copéret, P. M. Abdala, *JACS Au* **2024**, *4*, 1, 237, https://doi.org/10.1021/jacsau.3c00677.

[18] C. Copéret, *Acc. Chem. Res.* **2019**, *52*, 1697, https://doi.org/10.1021/acs.accounts.9b00138.